THE ASTROPHYSICAL JOURNAL, 436:L91–L94, 1994 November 20

AN *ASCA* OBSERVATION OF THE CASTOR SYSTEM

ERIC V. GOTTHELF,[1] LALIT JALOTA,[1,2] KOJI MUKAI,[1] AND NICHOLAS E. WHITE
Laboratory for High Energy Astrophysics, NASA/Goddard Space Flight Center, Greenbelt, MD 20771
Received 1994 August 1; accepted 1994 August 28

ABSTRACT

We report on a day-long *ASCA* broadband (1–10 keV) spectro-imaging observation of the X-ray emission from the Castor multibinary system. Significant flares were detected from both the flare star system YY Gem (Castor C) and from Castor AB located 73″ away. Using an optimal viewing geometry and image restoration techniques, we are able to spatially resolve the emission from the two X-ray components. Broadband flare activity from Castor AB is confirmed, and quiescent flux is detected. The quiescent spectrum of YY Gem is a complex blend of emission lines across the *ASCA* bandpass which requires multitemperature components or two-temperature variable metal-poor abundances (~5–10 below solar) to obtain a satisfactory fit to both the Mewe-Kaastra and Raymond-Smith models. The flare spectrum is consistent with an increase in the emissivity of the hotter component.

Subject headings: binaries: eclipsing — stars: abundances — stars: flares — stars: individual (Castor, YY Geminorum)

1. INTRODUCTION

The X-ray–bright Castor (α Geminorum) multibinary system is formed by three known optical components, each a spectroscopic binary pair. The main X-ray emission is located to component C, containing the flare star YY Gem (Gl 278 = Castor C) with a quiescent luminosity of $\log L_x = 29.63$ ergs s^{-1} at a distance of 14.7 pc (Caillault 1982). YY Gem is a well-studied optical and UV double-lined eclipsing binary ($P_{orb} = 0.81$ days) consisting of a (dM1e + dM1e) pair of $M_V = 8.37$; multiwavelength flares are observed at a phase-averaged rate of ~5 per day (Doyle & Mathioudakis 1990). Some 73″ away lies Castor A and B (collectively known as Castor AB), which consists of two A stars in a visual binary system with a separation of 2″–6″. Each A star is a single-line spectroscopic binary with orbital periods of 9.2 and 2.9 day for Castor A and B, respectively.

Early X-ray observations of the Castor system with the *Einstein* IPC were too short (2 × 0.6 hr) to distinguish quiescent from flare emission (flare timescale ~1 hr). Extended *EXOSAT* observation of this system (~35 hr over 3 days) revealed not only the expected X-ray flares from YY Gem, but also a flare from Castor AB (Pallavicini, Tagliaferri, & Stella 1990). Since A stars are not known to flare, this was an unexpected result, and it was presumed that the origin of the flare is one of the two unseen late-type companions. The *EXOSAT* data also suggested quiescent X-ray emission from Castor AB.

In this *Letter* we report preliminary results from a 1 day *ASCA* observation of the Castor system. This target was chosen not only because of its intrinsic interest as a flare star, but also to demonstrate that with careful planning *ASCA* can successfully distinguish two stars ~70″ apart, comparable to the ~1′ full width half-maximum (FWHM) of the telescope point-spread function (PSF).

2. OBSERVATIONS

The *ASCA* observatory is described in Tanaka et al. (1994). The instruments consist of two solid state imaging spectrometers (SIS), each consisting of four CCD chips, and two gas scintillation imaging spectrometers (GIS). Each detector is at the focus of its own imaging thin foil grazing incidence optics. The preliminary data reported herein are restricted to the SIS instrument which is more suitable to our image analysis. The spatial resolution of the GIS blurs the sharper features of the mirror PSF, while the SIS CCD pixels oversample the PSF by a factor of ~500. The SIS has a bandwidth of 0.4–10 keV and a resolution of ~2% at 6 keV. The *ASCA* observation of YY Gem began on 1993 October 25 at 14:26 UT and ended the following day at 15:50 UT. The SIS instrument was operated in 1-CCD mode giving a time resolution of 4 s and a FOV of 11′ × 11′. YY Gem was centered on the CCD chip, which corresponds to 7′ and 10′ off-axis for SIS0 and SIS1, respectively.

Observations of closely separated point sources ($\lesssim$1′) with *ASCA* are problematic. The PSF formed by ASCA's X-ray optics displays a distinctive four-lobe radial pattern, whose azimuthally average profile is characterized by a sharp core (FWHM ~ 50″ on-axis) and extended wings. The extended wings result in a half-power diameter of ~3′ and cause a significant degradation of the imaging capabilities. Simulations of *ASCA* images of close point sources predicted that Castor AB could be resolved from YY Gem by choosing an optimal roll angle which centers the image of Castor AB between lobes of YY Gem's PSF (Jalota, Gotthelf, & Zoonematkermani 1993). Image restoration techniques applied to these simulations were shown to help resolve the sources and enhance the effective image contrast.

3. ANALYSIS

The data were edited to exclude periods of unacceptable background contamination; and hot and flickering anomalous pixels were effectively removed using the CLEANSIS algorithm. This produced a mean count rate of 0.69 counts s^{-1} for SIS0 and 0.61 counts s^{-1} for SIS1 and resulted in a cleaned image dominated by YY Gem with a hint of excess flux at the putative location of Castor AB.

We then generated independent light curves of YY Gem and Castor AB in the 0.4–6 keV band using small apertures (50″ radius for YY Gem, containing ~50% of all YY Gem counts,

[1] Universities Space Research Association.
[2] Postal address: Tessella Support Services, 3 Vineyard Chambers, Abingdon, OX14 3PX, England.

and 30″/~30% for Castor AB); these light curves are shown in Figure 1. The aperture sizes were chosen as a compromise between the need to maximize the number of source photons and the need to exclude contamination by the other star. For YY Gem, background subtraction was not necessary (< 1/30 of source counts, including possible contribution of Castor AB), while for Castor AB (background about one-half of counts through the aperture) we have subtracted a background from an 30″ aperture on the opposite side of, and at the same distance from, YY Gem.

The YY Gem light curve (Fig. 1, *upper panel*) shows a quiescent counting rate of ~0.3 counts s^{-1} through the aperture, with an obvious flare peaking at 11:00 UT, October 26 and a possible flare sometime before 01:00 UT, October 26. Attitude jitter is estimated to be small enough (3″–10″) not to be a major contributor in the observed variability. There appears to be some reduction (~30%) in the X-ray flux during both primary and secondary eclipses, although quantitative assessment is made difficult by the variability. The Castor AB light curve (*lower panel*) reveals a mean quiescent rate of 0.023 counts s^{-1} and a flare at 04:00 UT, October 26. This flare is not seen in the YY Gem light curve, and likewise the YY Gem flares are not evident in the Castor AB light curve except as an increase in the noise level. This demonstrates that the strategy to place Castor AB in the shaded area of the PSF worked well.

We next accumulated SIS0 images for three time intervals corresponding to (*a*) the quiescent emission, (*b*) the flare from YY Gem, and (*c*) the flare from Castor AB. The smoothed images are shown in the upper panel in Figure 2 (Plate L2). Using the Lucy-Richardson deconvolution method (Lucy 1974; Richardson 1972) and the prelight Monte Carlo PSFs, the images were restored to a Gaussian equivalent resolution of the order of the central core of the PSF. The respective restored images are displayed in the lower panel of Figure 2. The cleaned quiescent image contains a total of 14 K counts and was restored using 50 iterations of the deconvolution algorithm. This resulted in a ≳ four-fold increase in contrast and Castor AB is detected at ≳10 σ level relative to the local background, confirming the quiescent X-ray flux from Castor AB. The YY Gem flare dominates the middle image, and the restoration does not help resolve Castor AB. The right-hand panel confirms the X-ray flare emission from Castor AB and shows that, for the source separation, it is possible to successfully deconvolve point sources with only 600 (YY Gem) and 1300 (Castor AB) counts.

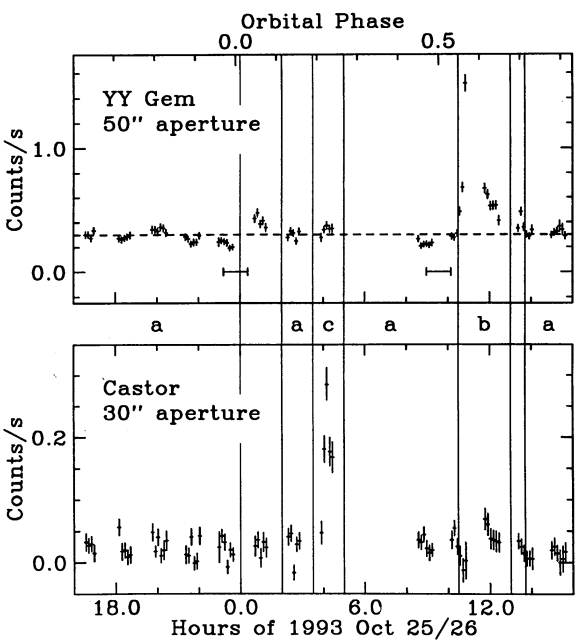

FIG. 1.—*ASCA* SIS light curves of YY Gem (50″ aperture; *upper panel*) and Castor AB (30″ aperture; *lower panel*). Counts from both SIS detectors have been summed into 480 s bins. The ordinate is time labeled in hours of 1993 October 25/26; it is also labeled in orbital phase of YY Gem (at top of the upper panel) using the GCVS ephemeris (Mallama 1980). For YY Gem, the horizontal bars indicate the estimate duration of the optical eclipse; the mean quiescent count rate of 0.3 counts s^{-1} is marked by the broken line. The vertical lines and the letters between plots correspond to the time intervals used for the images of Figure 2.

4. SPECTRAL RESULTS

In this *Letter* we will concentrate on the spectral data obtained by the best calibrated SIS instrument, SIS0. A spectrum was accumulated within a circular region with a radius of 4′ centered on the source. The intervals when there were flares or enhanced emission from either YY Gem (10:00–02:00 UT and 10:00–15:00 UT, October 26) or from Castor AB (03:00–06:00 UT, October 26) were excluded to obtain a spectrum of the YY Gem quiescent emission (with a ~10% contribution from Castor AB). A background was taken from the outer regions of the CCD chip, where counts from the outer wings of the mirror PSF are minimized. A total exposure time of 25,735 s was obtained. The source was detected in SIS0 between 0.4 and 7.0 keV. The spectral data were rebinned to have a minimum of 20 counts per channel.

The Raymond & Smith (1977) (R-S) and the Mewe-Kaastra (MEKA: Mewe, Gronenschild, & van den Oord 1985; Kaastra 1992) spectral models for emission from a plasma in thermal equilibrium with solar photospheric abundances were fitted to the spectra. A single-temperature model did not give a good fit (χ^2_ν of 13 for R-S and 8.4 for MEKA). For R-S, two-, three- and four-temperature (2T, 3T, and 4T) models gave unacceptable χ^2_ν of 4.92, 3.33, and 3.08. For MEKA the χ^2_ν decreases much faster to give 4.75, 2.15, 1.84, respectively. Adding a fifth component did not give any further improvement for either R-S or MEKA. The best-fitting 4T models and 90% uncertainties are given in Table 1. The best-fitting 4T-MEKA model is shown in Figure 3.

A 2T model gives a good fit to both R-S and MEKA if the abundance of the major line contributing elements in the *ASCA* SIS energy band are allowed to vary (Table 1). The 2T R-S variable abundance model gives a better fit than the 4T model, whereas for MEKA the two models give comparable χ^2 (see Table 1). The best fit to the data and the χ^2 residuals for the variable abundance MEKA model are shown in Figure 3. Table 1 lists the best-fit parameters and 90% uncertainties. There are substantial differences between the best-fit parameters for each model. The temperature of the cooler component is different by 0.2 keV, and the hotter component has a higher temperature in the MEKA model. The derived abundances are relative to solar as given by Anders & Grevesse (1989). The best-fit values show the same trends in both the MEKA and R-S models and are a factor of 2–10 below the solar photospheric value. The most extreme is iron, which is only 0.09–0.15 of the solar photospheric value. A continuous emission measure distribution from solarlike loops (cf. Schmitt et al. 1990) using the MEKA plasma code did not give an acceptable

PLATE L2

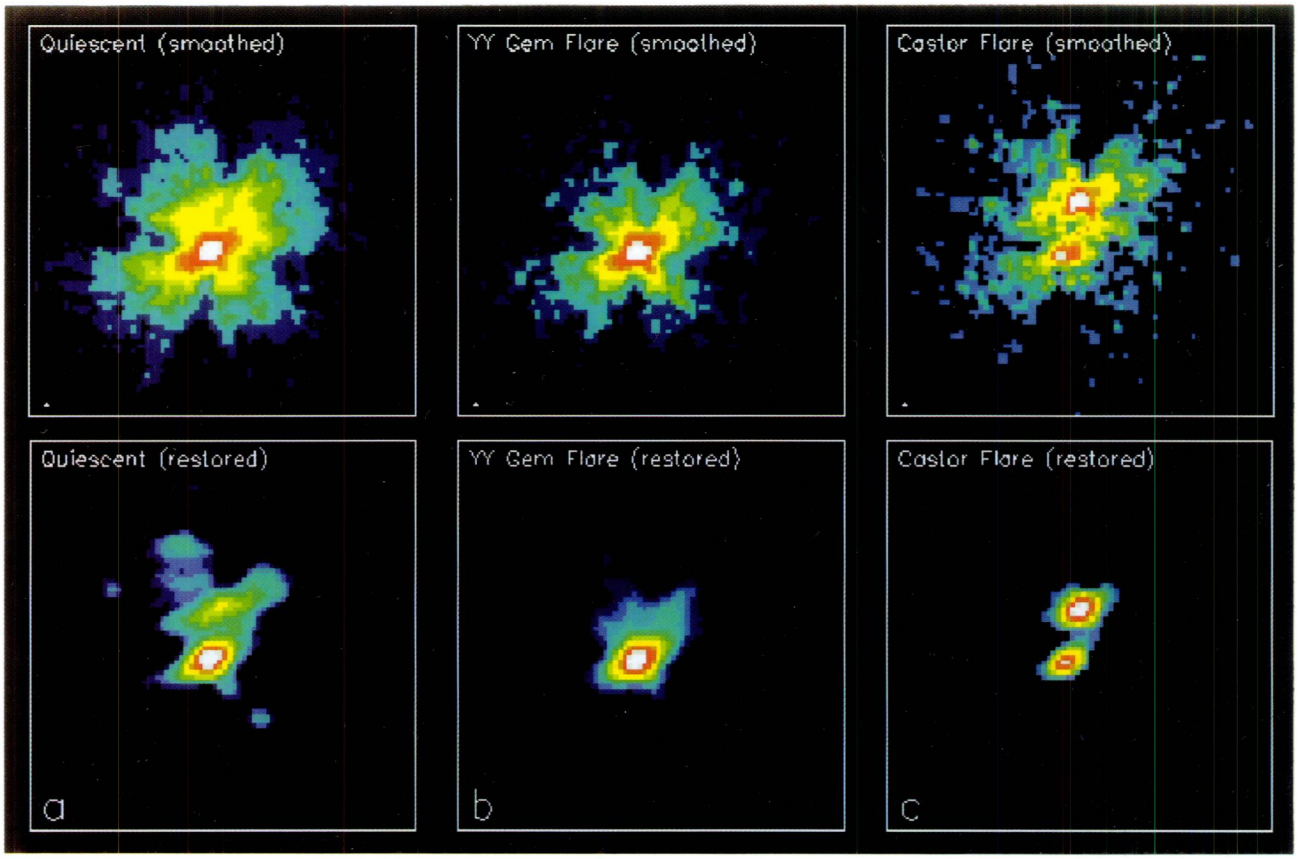

FIG. 2.—*ASCA* SIS-0 images of YY Gem and Castor AB accumulated in three time intervals corresponding to (*left*) the quiescent emission; (*middle*) the flare from YY Gem; and (*right*) the flare from Castor AB. The upper panel displays the smoothed, cleaned images. The X pattern of the mirror PSF is evident. The lower panel shows the respective images restored using the Lucy-Richardson deconvolution method (see text). Panel (*a*) shows unambiguous detection of quiescent emission from Castor AB as well as YY Gem (*bottom source*); the light blue contour is at the noise level. In (*b*) The YY Gem flare dominates the Castor emission, which is unresolvable. In (*c*) the emission from the Castor flare is greater than the quiescent flux from YY Gem. The distance between YY Gem and Castor is $\sim 70''$. Each image is displayed with logarithmic scaling, and the color scale is normalized to the peak intensity of that image.

GOTTHELF et al. (see 436, L92)

TABLE 1

SPECTRAL FITS TO THE *ASCA* SIS0 YY GEMINORUM QUIESCENT SPECTRUM

Parameter	2T-MEKA	2T–R-S	4T-MEKA	4T–R-S
χ^2	1.72	1.56	1.84	3.08
EM_1 (cm^{-3})	3.3×10^{52}	3.0×10^{52}	6.30×10^{52}	3.0×10^{52}
kT_1 (keV)	0.60 ± 0.04	0.38 ± 0.03	0.06 ± 0.03	0.08 ± 0.03
EM_2 (cm^{-3})	3.2×10^{51}	1.2×10^{52}	2.0×10^{51}	3.7×10^{51}
kT_2 (keV)	3.7(2.0, ∞)	1.52 ± 0.15	0.23 ± 0.03	0.28 ± 0.01
EM_3 (cm^{-3})	...	...	7.6×10^{51}	5.4×10^{51}
kT_3 (keV)	...	...	0.68 ± 0.04	0.89 ± 0.02
EM_4 (cm^{-3})	...	...	4.2×10^{51}	4.2×10^{51}
kT_4 (keV)	...	...	2.7(2.3, 3.4)	2.8(2.5, 3.4)
log L_x (flare)[a]	29.46	29.36(30.0)	29.65(30.0)	29.37
N (1.12E−4)	<0.6	<0.18	1.0	1.0
O (8.51E−4)	0.4(0.6, 0.3)	0.15 ± 0.10	1.0	1.0
Ne (1.23E−4)	0.61 ± 0.17	0.37 ± 0.15	1.0	1.0
Mg (3.80E−5).....	0.16 ± 0.10	0.17 ± 0.13	1.0	1.0
Si (3.55E−5)	0.25 ± 0.15	0.45 ± 0.17	1.0	1.0
S (1.62E−5)	0.29(0.0, 0.75)	<0.5	1.0	1.0
Ar (3.63E−6).....	<2.0	<0.9	1.0	1.0
Ca (2.29E−6)	<1.0	<0.4	1.0	1.0
Fe (4.68E−5).....	0.15(0.04, 0.08)	0.09 ± 0.03	1.0	1.0
Ni (1.78E−6).....	<0.3	2.5 ± 0.7	1.0	1.0

[a] log L_x ergs s^{-1} in the *Einstein* IPC 0.4–4.5 keV bandpass, for $d = 14.7$ pc.

fit (χ^2_ν of 6.3). The best-fitting hydrogen column density for all the trial models was zero, although values up to a few 10^{18} cm^{-2} could not be excluded.

The large flare seen from YY Gem rises to maximum within ~100 s and is associated with an overall hardening of the spectrum. Unfortunately there is a data gap during most of the decay which last about 4000 s. There is ~550 s of data during the peak. A flare spectrum was accumulated for this interval. To investigate the flare spectrum itself, the quiescent spectrum was subtracted as background. When fitted to a single-component model a temperature of 1.3 keV is obtained for R-S and 2.5 keV for MEKA. In both cases the χ^2 is poor with values of 2.2 for both models. Allowing the abundances of all the elements to vary together improved the fit slightly, giving an abundance of 0.3 solar, but it was still unacceptable. We also made a simultaneous fit to the quiescent spectrum and the flare spectrum, using the same source-free background, for both the 4T and variable abundance 2T models, keeping the temperatures fixed at their best-fitting quiescent values. In both cases a χ^2_ν of order 1 was obtained if the normalization of the highest temperature component was allowed to increase. This is consistent with the flare being caused simply by an increase in the emission measure of the hotter component.

We extracted the spectrum of Castor AB from the SIS0 data, in the manner described for the light curve. The resultant spectrum (320 net counts) can be fitted by a 2T R-S model (the choice of model is not unique, although this is a significant improvement over a 1T R-S model), and gives temperatures of

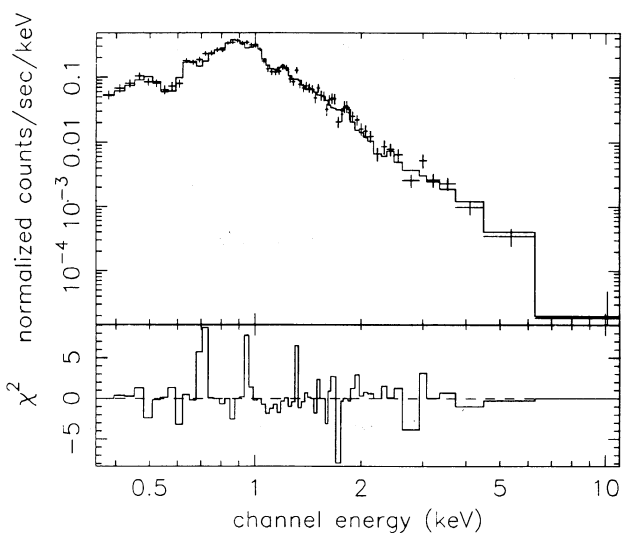

FIG. 3*a*

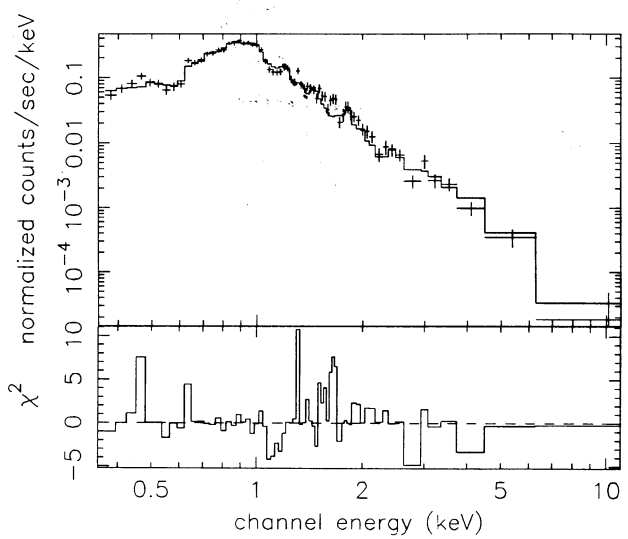

FIG. 3*b*

FIG. 3.—The best fit to the SIS0 spectra for a variable abundance two-temperature MEKA model (*a*) and four-temperature MEKA model (*b*). The residuals to each best-fitting model are given in the lower panels as the χ^2 contributions to each bin.

0.25 ± 0.15 and 0.95 ± 0.25 keV with a χ^2_ν of 0.65 (quoted errors are nominal 90% confidence limits from counting statistics; systematic errors, due to the difficulties of background subtraction, are not included). The flare spectrum of Castor AB is then consistent with an increase in emission measure of the ~ 1 keV plasma, within uncertainties. The derived luminosity in the *Einstein* IPC bandpass, assuming a distance of 14.7 pc, is $\log L_x = 28.6$ ergs s^{-1} for the quiescent emission and $\log L_x = 29.3$ ergs s^{-1} during the flare interval.

5. DISCUSSION

The spectrum of the quiescent emission from YY Gem can be fitted by two possible models: (1) a 4T photospheric abundance MEKA model or (2) a 2T R-S or MEKA model where the abundances are a factor of 5–10 below the solar photospheric value. The latter model is quite similar to that found by Swank & Johnson (1982) for Wolf 630AB and is also similar to the spectra of RS CVn stars (e.g., White et al. 1994). In this model the high-temperature component dominates the spectrum above 1 keV. The lower temperature is responsible for a complex of iron L emission at 0.8–1 keV. The 4T MEKA model is a new possibility for these systems. Such models have been excluded for the RS CVn systems, where the statistical quality of the data are much higher. For this YY Gem observation the signal-to-noise ratio around 6–7 keV is not sufficient to measure the strength of the iron K-line emission, which would be a crucial test in differentiating between the two models.

Schmitt et al. (1990) made a comprehensive survey of the X-ray spectra of M dwarfs. In those systems where sufficient counts were accumulated two-temperature spectra are required, but with typical temperatures of 0.26 keV and 2.6 keV. Swank & Johnson (1982) find values of 0.54 and >0.7 keV from the *Einstein* SSS (see also Agrawal, Rao, & Sreekantan 1986). The different temperature pairs reported here of 0.38 and 1.5 keV from the R-S model and 0.6 and 3.7 keV for the MEKA model illustrate that systematic uncertainties in the plasma codes dominate, and that all these determinations are consistent. We rule out continuous emission measure models based on solar loops. It has been suggested that the quiescent emission from flare stars like YY Gem may be the sum of continuous microflaring activity, that is unresolved (cf. Butler et al. 1986). The hottest component determined for both the 2T and 4T models has a temperature consistent with the 1.7–3.5 keV range seen in flares from flare stars (Pallavicini et al. 1990), consistent with this component being caused by the superposition of flares.

Our results of image restoration of *ASCA* data agrees well with preflight simulations. We verified that the deconvolution technique can successfully enhance *ASCA* images by increasing the effective spatial resolution and the image contrast, and by removing much of the strong azimuthal structure. The deconvolved images, as well as the light curves, confirm both quiescent and flare X-ray emission from Castor AB, as suspected by Pallavicini et al. (1990). However, the nature of this emission is unresolved by the spectral data due to poor statistics, but the flare episode suggests a late-type system similar to YY Gem.

The authors would like to thank the entire *ASCA* team, particularly those who are involved in the day-to-day operation of the satellite, for making this observation possible. We are grateful to the referee, J.-P. Caillault, for helpful comments.

REFERENCES

Agrawal, P. C., Rao, A. R., & Sreekantan, B. V. 1986, MNRAS, 219, 225
Anders, E., & Grevesse, N. 1989, Geochim. Cosmochim. Acta, 53, 197
Butler, C. J., Rodonò, M., Foing, B. H., & Haisch, B. M. 1986, Nature, 321, 679
Caillault, J. P. 1982, AJ, 87, 558
Doyle, J. G., & Mathioudakis, M. 1990, A&A, 227, 130
Jalota, L., Gotthelf, E. V., & Zoonematkermani, S. 1993, Proc. SPIE, 1945, 453
Kaastra, J. S. 1992, An X-Ray Spectral Code for Optically Thin Plasmas (SRON-Leiden Report)
Lucy, L. 1974, AJ, 79, 745
Mallama, A. D. 1980, PASP, 92, 468
Mewe, R., Gronenschild, E. H. B. M., & van den Oord, G. H. J. 1985, A&A, 62, 179
Pallavicini, R., Tagliaferri, G., & Stella, L. 1990, A&A, 228, 403
Raymond, J. C., & Smith, B. W. 1977, ApJS, 35, 419
Richardson, W. H. 1972, J. Opt. Soc. Am., 62, 55
Schmitt, J. H. M. M., Collura, A., Sciortino, S., Vaiana, G. S., Harnden, F. R., & Rosner, R. 1990, ApJ, 365, 704
Swank, J. H., & Johnson, H. M. 1982, ApJ, 259, L67
Tanaka, Y., Inoue, H., & Holt, S. S. 1994, PASJ, 46, L37
White, N. E., et al. 1984, PASJ, 46, L97

Note added in proof.—After the acceptance of this paper, we have become aware of the paper by Schmitt, Gudel, & Predehl (A&A, 287, 843 [1994]), which discusses *ROSAT* and VLA observations of the Castor system. Their analysis of *ROSAT* data generally confirms the conclusions we have independently derived from *ASCA* data. The one major difference is the derived luminosity of Castor AB: their value, $\log L_x = 29.2$ (in *ROSAT* band), is 4 times higher than the quiescent luminosity ($\log L_x = 28.6$ in the *Einstein* band) that we derive from the *ASCA* data and is in better agreement with our flare value ($\log L_x = 29.3$). The difference cannot be due to minor differences in the distance adopted; it could be due to uncertainties associated with conversion from *ROSAT* HRI count rate to luminosity, or because the HRI observation caught Castor AB flare(s). Schmitt et al. (1990) pointed out that, given dynamical constraints, the unseen companion to Castor A will have to be exceptionally X-ray active to have a quiescent X-ray luminosity they derive; therefore, the unseen companion model for the origin of Castor AB X-rays has a serious problem. This model appears to be viable once again, with our measurement of the quiescent luminosity.